Experimental Design for Negative Triaxialities: Ductile Fracture Under Combined Uniaxial Tension and Hydrostatic Pressure

Robert L. Lowe, Luke D. Hoover, and Christopher A. Negri
Department of Mechanical and Aerospace Engineering, University of Dayton, Dayton, OH 45469

Abstract

Many modern continuum-scale approaches for modeling the ductile fracture of metals regard the equivalent plastic strain at fracture as a function of the stress triaxiality and Lode parameter, a pair of invariant-based quantities that together characterize the three-dimensional state of stress at a point. Generally, these ductile fracture models (whether parameterized or tabulated) are calibrated using standard mechanical tests, e.g., notched axisymmetric (round), plane stress (thin), and plane strain (thick) specimens subjected to tensile loading. However, these standard tests are only able to capture a limited window of stress states, leaving potentially important "regions" of the ductile fracture model unpopulated with experimental data. For instance, although previous research has suggested that fracture will not occur below a triaxiality of -0.33 (the "cut-off" value), recent ballistic impact simulations involving 0.5-inch-thick titanium Ti-6Al-4V target plates predicted large negative (compressive) triaxialities in the vicinity of the adiabatic shear band. These results not only suggest the potentially unanticipated importance of the negative triaxiality (compressive) region of Lode-triaxiality stress space, but also the need to experimentally revisit previous interpretations of the "cut-off" value of the triaxiality. As a first step, this paper presents a novel physical interpretation of the Lode parameter = 1 (constant) meridian over a range of triaxialities, spanning positive (tensile) to negative (compressive). Guided by this physical insight, ductile fracture experiments that employ hydrostatic pressure superposed on uniaxial tension are proposed and numerically simulated in LS-DYNA®, with initial efforts focusing on 2024-T351 aluminum. Our numerical simulations provide a promising "virtual" proof-of-concept demonstrating that stress triaxiality can be tuned (at constant Lode parameter) by adjusting the magnitude of the applied pressure, allowing a wide range of stress states to be accessed through a single experimental test setup.

Introduction

Modeling and simulating the impact physics of jet engine debris striking the engine case – or, in rare cases, the aircraft structure (e.g., fuselage or wings) – during a fan blade-out or rotor-burst event is notoriously challenging [1,2]. In the case of metals, the complex impact-penetration physics involves high strain rates, steep temperature gradients, large plastic deformations, progressive damage, and ultimately ductile fracture, all of which must be taken into account in the analysis. Notably, the ductile fracture model employed in the finite-element analysis must be capable of predicting multiple potential failure modes (e.g., plugging and petaling), which are intimately related to the impact conditions (e.g., projectile and target material properties, geometry, relative orientation, and impact speed) and subsequent state of stress at impact [1,2]. For instance, in ballistic impact tests, thin-sheet failure is often tension-dominated and characterized by radial tearing of the impact zone into petals (petaling), whereas thick-plate failure is often shear-dominated and characterized by the formation of a coin-like plug (plugging) [1,2]. Thus, different impact conditions lead to different states of stress at impact and, consequently, different failure modes, all of which must be faithfully captured by the ductile fracture model.

The primary microscopic mechanism driving ductile fracture in metals is the nucleation, growth, and coalescence of voids [3,4]. Ductile fracture has been modeled at different length scales; our interest in this paper is in continuum-scale phenomenological models, which are widely used in commercial finite-element codes for structural-level analysis. Phenomenological approaches, in contrast to micromechanics-based approaches (see, for instance, Refs. [5-9]), are inspired by – but do not explicitly model – void nucleation, growth, and coalescence. Perhaps the most famous phenomenological ductile fracture model is that of Johnson and Cook [10], which

provides a mathematical relationship between the equivalent plastic strain at fracture (a common measure of ductility) and the stress triaxiality (defined as the ratio of the mean (hydrostatic) stress to the effective (von Mises) stress). The Johnson-Cook model was motivated by the pioneering experiments of Hancock and Mackenzie [11], who showed that the equivalent plastic strain at fracture decreases exponentially with increasing triaxiality. The relationship between stress triaxiality and ductility was further explored in Refs. [12-17]. However, more recent experimental investigations have conclusively shown that triaxiality alone is insufficient to model the ductile fracture of metals over the full range of potential stress states. This limitation was first observed by Bao and Wierzbicki [14] and later confirmed through the experimental work of Barsoum and Faleskog [18], who found that the ductility depends on the state of stress through both the triaxiality and the Lode parameter. Ductile fracture models incorporating both stress triaxiality and Lode parameter dependence can be found in Refs. [19-26]. Experimental work investigating this dependence can be found in Refs. [27-35].

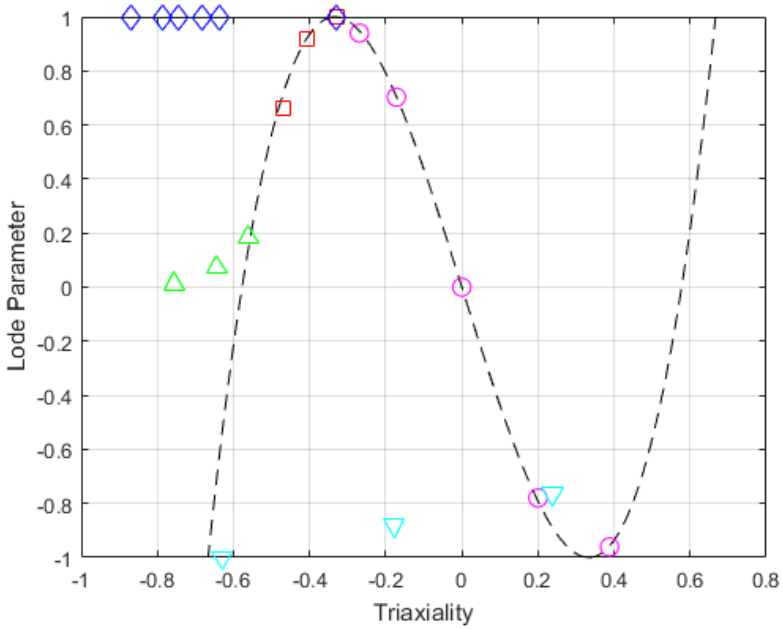

Figure 1: Stress states investigated in the ductile fracture experiments performed by Seidt [27,31] on 2024-T351 aluminum. Blue diamonds denote tension tests on axisymmetric (round) specimens; green triangles denote tension tests on plane strain (thick) specimens; red squares denote tension tests on plane stress (thin) specimens; magenta circles denote tension-torsion, torsion, and compression-torsion tests; and cyan triangles denote punch tests. Figure adapted from Ref. [45]. **Note that the triaxialities in this figure are defined following Eq. (4), the form used in LS-DYNA, which differs from the standard definition (Eq. (3)$_1$) by a minus sign.**

2024-T351 aluminum alloy is an important aerospace metal used in critical aircraft components such as fuselage skins, wing skins, and engine cowlings. A number of experimental studies focusing on the ductile fracture of 2024-T351 aluminum have been performed following the approach popularized by Wierzbicki et al. (described, for instance, in Ref. [14]). Among these, perhaps the most comprehensive experimental program on 2024-T351 was performed by Seidt [27,31], which included tension tests on notched axisymmetric (round), plane stress (thin), and plane strain (thick) specimens as well as tension-torsion, torsion, and compression-torsion tests on thin-walled tube specimens; refer to Fig. 1. At present, a large region of Lode-triaxiality space in Fig. 1 remains unpopulated with experimental data. Of particular interest in this paper is the negative triaxiality (compressive) region. Although previous research [36] has suggested that fracture will not occur below triaxialities of -0.33 (the "cut-off value"), recent ballistic impact simulations involving 0.5-inch Ti-6Al-4V target plates predicted large negative triaxialities (between -0.2 and -5.0) in the vicinity of the adiabatic shear band [37]. Several recent experiments [38-41] exploring negative triaxialities further call into question this previous "cut-off" value.

Together, these findings suggest the potentially unanticipated importance of the negative triaxiality (compressive) region of Lode-triaxiality space, which remains largely unpopulated with experimental data for aerospace metals such as 2024-T351 aluminum.

To begin to address this need, the primary goal of this paper is to present an experimental approach for characterizing the ductile fracture of 2024-T351 aluminum for triaxialities ranging from 0.33 (tensile) to -0.66 (compressive) at a constant Lode parameter of 1. We propose to accomplish this through experiments that investigate ductile fracture under combined uniaxial tension and hydrostatic pressure. Mechanical testing under large hydrostatic pressure (on the order of hundreds or thousands of MPa) has been extensively investigated, summarized nicely in the seminal work of Bridgman [42] and the more recent review by Lewandowski and Lowhaphandu [43]. However, to the best of our knowledge, we may be the first to recognize that, by superposing hydrostatic pressure on a conventional "plane stress" mechanical test (e.g., uniaxial tension), the baseline triaxiality can be "tuned" (at any constant Lode parameter) by simply adjusting the pressure – in essence, rendering a ductile fracture experiment with any desired (increasingly negative) triaxiality, up to the (Lode-dependent) "cut-off" beyond which no fracture will occur. This concept, with its embedded tunability, shows great promise for accessing numerous stress states with a single test setup.

Accessing Stress States with Negative Triaxialities: Combined Tension and Pressure

Consider the following dimensionless Cauchy (true) stress tensor, whose Cartesian components are

$$[\boldsymbol{\sigma}] = \begin{bmatrix} -a & 0 & 0 \\ 0 & -a & 0 \\ 0 & 0 & 1-a \end{bmatrix} \tag{1}$$

The state of stress (1) represents a combined state of uniaxial tension and hydrostatic pressure (compression), with all components normalized by the uniaxial tensile stress σ_{zz}. The non-dimensional parameter a in Eq. (1), defined by

$$0 \leq a = \frac{p}{\sigma_{zz}} \leq 1 \tag{2}$$

quantifies the competition between hydrostatic pressure p and uniaxial tension σ_{zz}. The triaxiality σ^* and Lode parameter μ follow from their standard definitions:

$$\sigma^* = \frac{\sigma_m}{\bar{\sigma}} = \frac{1}{3} - a \qquad \mu = \frac{27}{2}\frac{J_3}{\bar{\sigma}^3} = 1 \tag{3}$$

where $\sigma_m = \frac{1}{3}(\mathrm{tr}\,\boldsymbol{\sigma})$ is the mean stress, $\bar{\sigma} = \sqrt{3J_2}$ is the von Mises (equivalent) stress, and J_2 and J_3 are the second and third principal scalar invariants of the deviatoric stress $\mathbf{S} = \boldsymbol{\sigma} - \sigma_m\mathbf{I}$. By adjusting the dimensionless parameter $0 \leq a \leq 1$ (i.e., increasing the relative magnitude of the applied hydrostatic pressure), the triaxiality σ^* can be tuned at constant Lode parameter ($\mu = 1$) from $\sigma^* = 0.33$ (uniaxial tension) to $\sigma^* = -0.66$ (equi-biaxial compression); refer to Fig. 1. We could, of course, admit stress states generated by allowing $a \geq 1$; however, it is hypothesized that fracture will not occur for 2024-T351 aluminum in these compression-dominated stress states, although this remains to be confirmed by experiments.

Experimental Design and Numerical Simulations

Based on the physical insight obtained in the previous section, we embark on designing experiments where the fracture site in the test coupon/specimen is proportionally loaded to fracture under a state of combined uniaxial tension and hydrostatic compression. The target strain rate is 0.01 1/s (quasi-static). Accordingly, the proposed experimental setup consists of a standard plane stress (thin) or axisymmetric (round) test coupon subjected to combined uniaxial tension and hydrostatic pressure. The uniaxial loading is applied to the specimen by a servohydraulic universal testing machine, and the hydrostatic pressure is applied either pneumatically or hydraulically. Similar setups have been developed previously and are summarized, for instance, in Refs. [42,43]. In what follows, through proof-of-concept "virtual" combined tension-pressure tests on 2024-T351 aluminum, we confirm that stress triaxiality can be tuned (at constant Lode parameter) by adjusting the magnitude of the applied pressure, allowing a wide range of stress states to be accessed through a single experimental test setup.

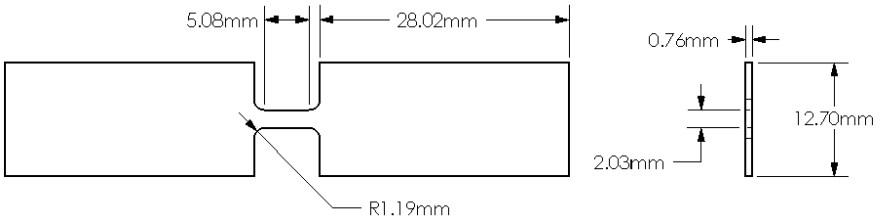

Figure 2: 0.76-mm-thick plane stress test coupon used in our experimental design [32].

Our candidate specimen geometry is the 0.76-mm-thick plane stress coupon shown in Fig. 2, used in previous ductile fracture experiments for Ti-6Al-4V [32]. Three-dimensional solid models of the specimen geometry were rendered in SolidWorks (2019 version, Dassault Systemes, Waltham, MA). A finite-element mesh was generated using the grid-generation software HyperMesh (2017.1 version, Altair, Troy, MI); see Fig. 3. Following standard practice in experimental mechanics [44], about 75% of the elements in the shoulder tabs are gripped and thus modeled as rigid elements, denoted by light gray shading in Fig. 3. Numerical simulations were performed in the commercial finite-element suite LS-DYNA (version R10.1.0, Ansys/LST, Livermore, CA). Three-dimensional, constant-stress, 8-node, solid hex elements (ELFORM = 1) were used in the simulations. The finite-element model contained about 72,000 elements with a characteristic mesh size of 0.2 mm. The element density in the specimen gage was 10 across the width and 4 through the thickness, with each element's aspect ratio approaching 1:1. To account for the tendency of under-integrated elements to hourglass, stiffness-based hourglass control (IHQ = 6) was employed with an hourglass coefficient QH = 0.1. Hourglass energies imposed by the hourglass control algorithm were found to be acceptably low in all simulations.

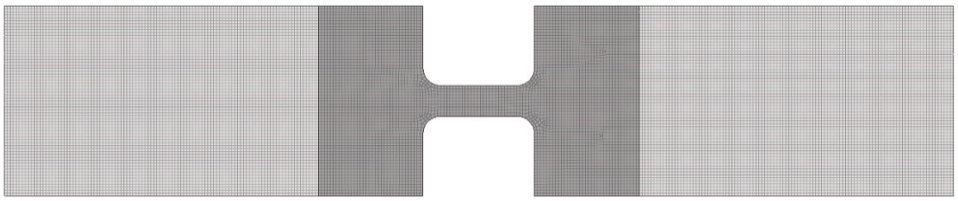

Figure 3: Finite-element mesh of the specimen used in our experimental design. The finite-element model contains about 72,000 elements with a characteristic mesh size of 0.2 mm. Light gray shading denotes the gripped sections of the shoulder tabs.

Our candidate metal is 2024-T351 aluminum. The gripped sections in the shoulder tabs of the 2024-T351 aluminum specimen (denoted by light gray shading in Fig. 3) were modeled as rigid using the *MAT_20 material card in the LS-DYNA material library. The ungripped shoulder and gage sections of the coupon specimen

(denoted by dark gray shading in Fig. 3) were modeled using the *MAT_224 material card. In *MAT_224, isotropic linear elastic deformation is characterized in a parametrized fashion by specifying two elastic constants, Young's modulus and Poisson's ratio. After yield, thermo-viscoplastic deformation is characterized through user-input hardening curves (effective true stress vs. effective true plastic strain) at different temperatures and strain rates. Using these curves, a J2 (von Mises) yield surface is constructed numerically and used internally by the code. In this work, we used a publicly available version of *MAT_224 that was calibrated by Park et al. [45] to an extensive set of experimental data for 2024-T351 aluminum.

Uniform pressures of 0 MPa, 300 MPa, and 600 MPa were applied to the exterior surface of the ungripped shoulder and gage sections of the specimen in Fig. 3 using the *LOAD_SEGMENT_SET card. A *SEGMENT_SET was defined using the graphical user interface in LS-PrePost® (version 4.7.9, Ansys/LST, Livermore, CA) by first selecting Model and Part → Create Entity → Create → Set Data. Then, in the selection tool, "Pick" and "By Part" were selected, and the "3DSurf" box was checked so that only elements with surfaces on the exterior boundary of the specimen populated the *SEGMENT_SET. The pressure was initiated as a step function at time $t = 0$, synchronous with the onset of the uniaxial actuator.

The motion of the rigid gripped sections of the specimen was restricted using the center of mass constraint option (CMO = 1) in *MAT_20. For the gripped section fixed to the universal testing machine, we set the constraint parameters CON1 = CON2 = 7 to constrain all translational and rotational degrees of freedom. The gripped section driven by the uniaxial actuator was constrained using CON1 = 5, CON2 = 7 so that only axial translation was permitted. Using the *BOUNDARY_PRESCRIBED_MOTION_RIGID card, a constant actuator speed was prescribed. For all of our simulations, we used an "artificial" actuator speed of 1 m/s, following the procedure described by Haight et al. [37] and summarized in what follows. (Note that the adjective "artificial" refers to the dichotomy between the imposed actuator speed (1 m/s) and the target strain rate (0.01 1/s), which are incompatible.) By suppressing all hardening curves in *MAT_224 except that of the target strain rate (0.01 1/s) at room temperature, the plasticity model was rendered rate-independent. This allowed us to impose a substantially larger ("artificial") actuator speed in the simulations than would be used in a true quasi-static experiment, greatly reducing computational cost. A caveat is that the imposed actuator speed must not introduce inertial effects: a uniaxial tension experiment conducted at a strain rate of 0.01 1/s is quasi-static. The absence of dynamic effects was confirmed by running simulations over a range of "artificial" loading speeds (e.g., 10 m/s, 1 m/s, 0.1 m/s), and identifying where the simulation results (e.g., force-displacement curves) first diverge. For all of our simulations, 1 m/s was the largest acceptable actuation speed.

All of our simulations terminated normally, generally in well under 30 minutes, using a shared-memory parallel (SMP) version of LS-DYNA running on 8 CPUs. Figures 4, 6, and 8 are contour plots of the triaxiality, Lode parameter, and damage – just prior to fracture – at pressures of 0 MPa, 300 MPa, and 600 MPa. Figures 5, 7, and 9 are history plots of the triaxiality, Lode parameter, and damage – in the first element to fail (erode) – at pressures of 0 MPa, 300 MPa, and 600 MPa. **It is critical to note that LS-DYNA employs a different definition of triaxiality than is standard, i.e.,**

$$\sigma^* = -\frac{\sigma_m}{\bar{\sigma}} \tag{4}$$

With this definition, the triaxiality is -0.33 in a uniaxial tension test, 0.33 in a uniaxial compression test, and 0.66 in an equi-biaxial compression test. **Consequently, the triaxialities in Figs. 4-9 differ from the standard definition by a minus sign.** Our metrics for a "successful" test include (a) obtaining targeted values of triaxiality and Lode parameter (i.e., triaxialities from 0.33 to -0.66 (standard definition) or -0.33 to 0.66 (LS-DYNA

definition), (b) maintaining these targeted values (i.e., proportional loading) as damage begins to accumulate, and (c) ensuring uniformity of these values spatially within the specimen gage (i.e., test repeatability).

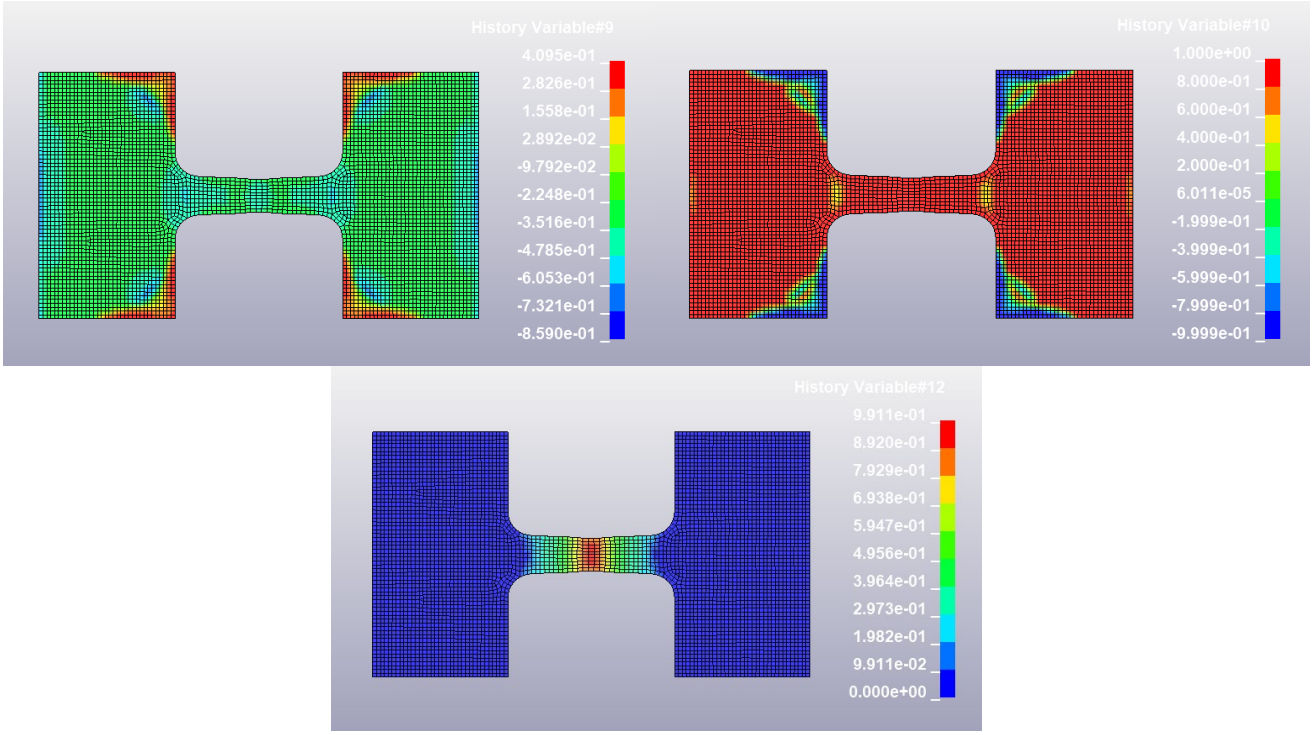

Figure 4: Applied pressure = 0 MPa. Contour plots of triaxiality (upper left; LS-DYNA definition), Lode parameter (upper right), and damage (bottom) immediately before fracture. Note the region of localized damage at the geometric center of the specimen's gage section.

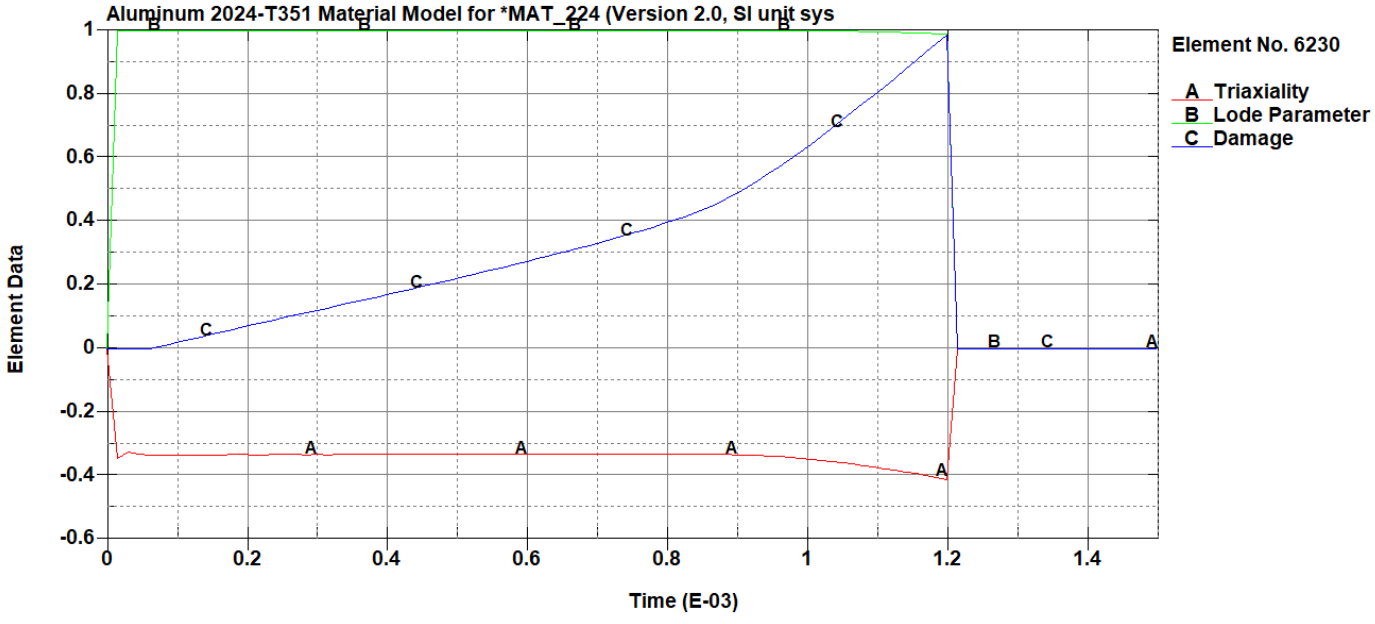

Figure 5: Applied pressure = 0 MPa. History plot of triaxiality (red), Lode parameter (green), and damage (blue) in the first element to fail (erode), located at the geometric center of the specimen's gage section. After 10% damage, the average triaxiality is about -0.33 (LS-DYNA definition) or 0.33 (standard definition), and the average Lode parameter is about 1.

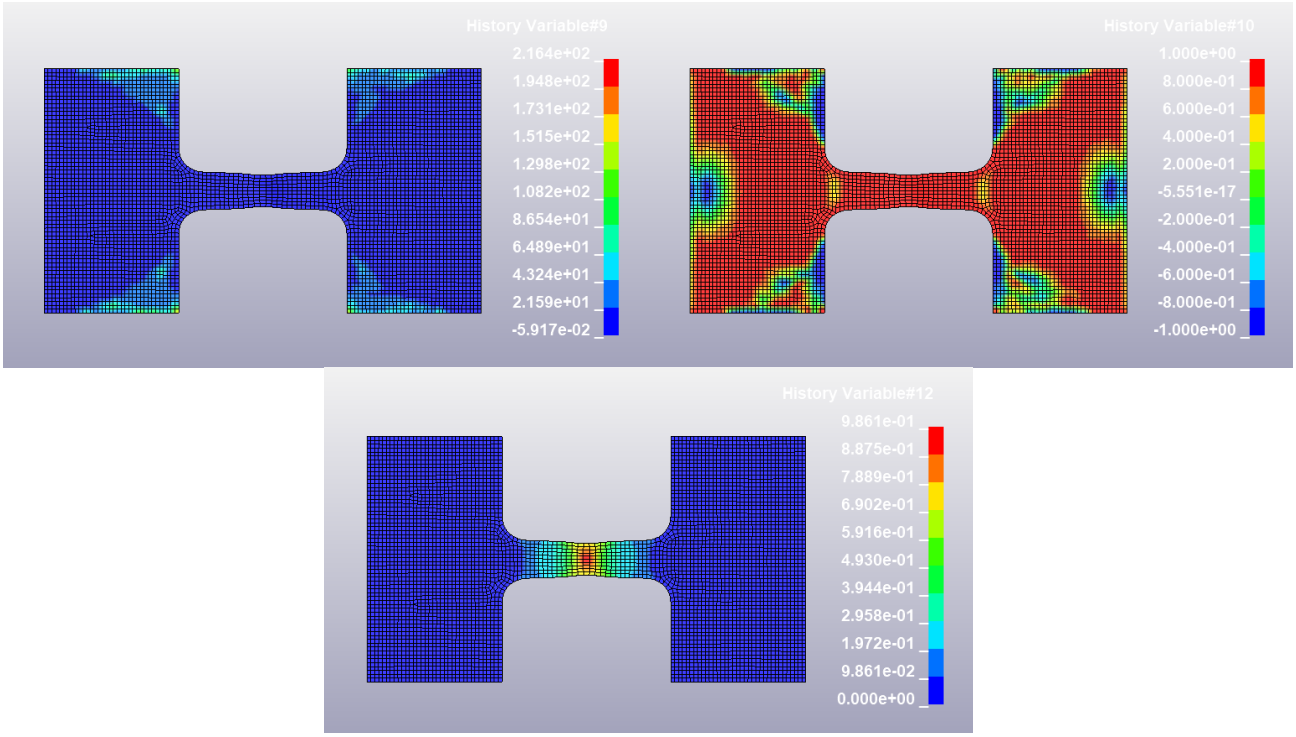

Figure 6: Applied pressure = 300 MPa. Contour plots of triaxiality (upper left; LS-DYNA definition), Lode parameter (upper right), and damage (bottom) immediately before fracture. Note the region of localized damage at the geometric center of the specimen's gage section.

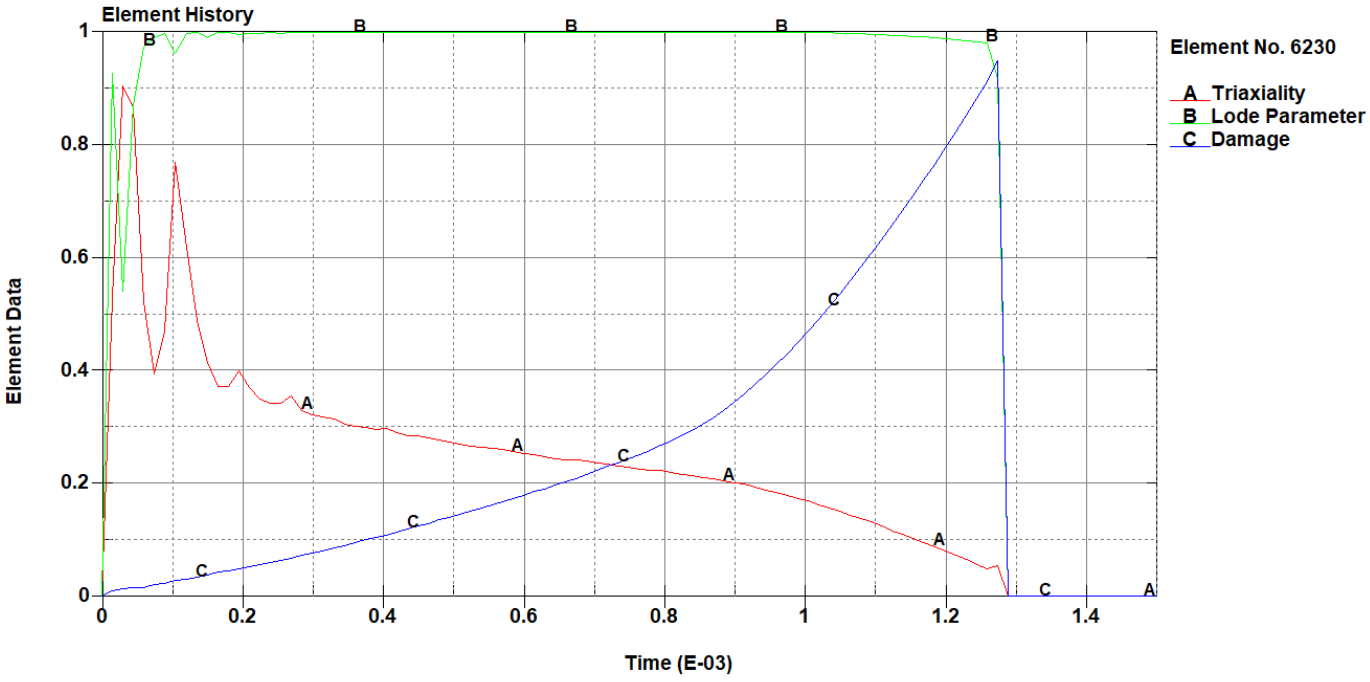

Figure 7: Applied pressure = 300 MPa. History plot of triaxiality (red), Lode parameter (green), and damage (blue) in the first element to fail (erode), located at the geometric center of the specimen's gage section. After 10% damage, the average triaxiality is about 0.2 (LS-DYNA definition) or -0.2 (standard definition), and the average Lode parameter is about 1.

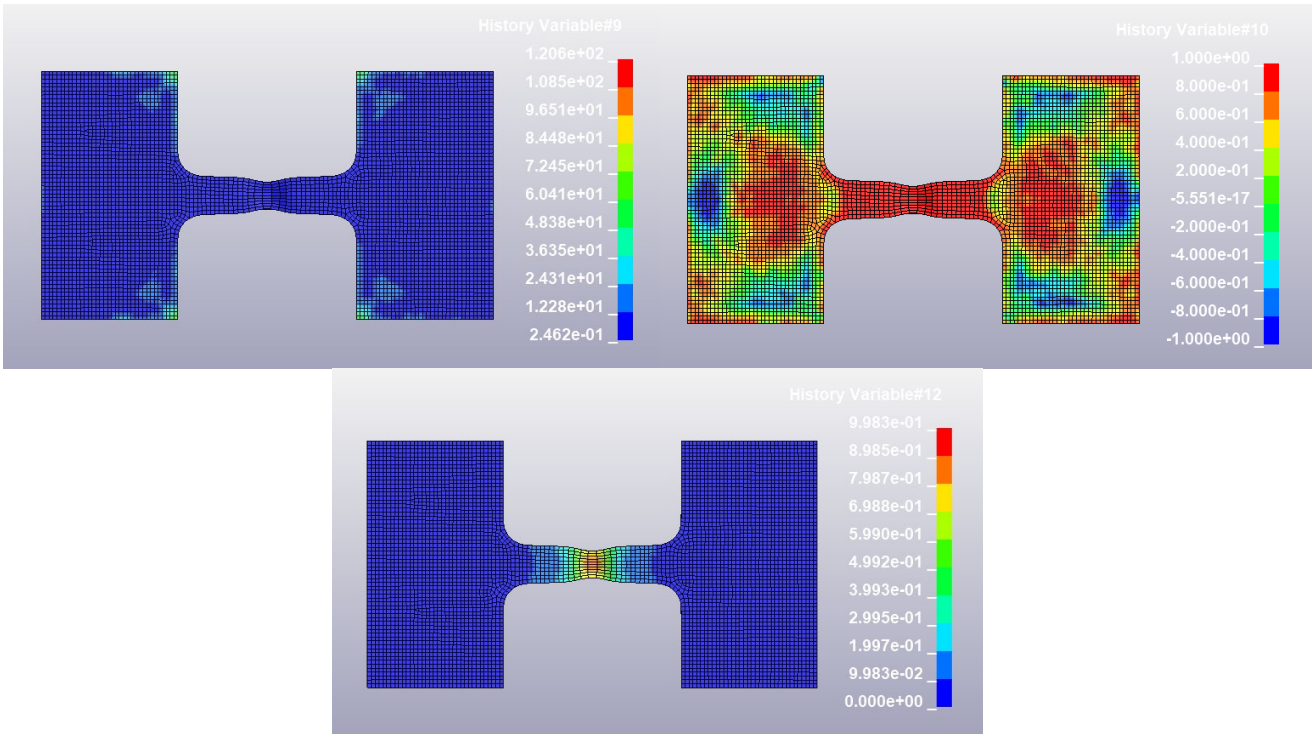

Figure 8: Applied pressure = 600 MPa. Contour plots of triaxiality (upper left; LS-DYNA definition), Lode parameter (upper right), and damage (bottom) immediately before fracture. Note the region of localized damage at the geometric center of the specimen's gage section.

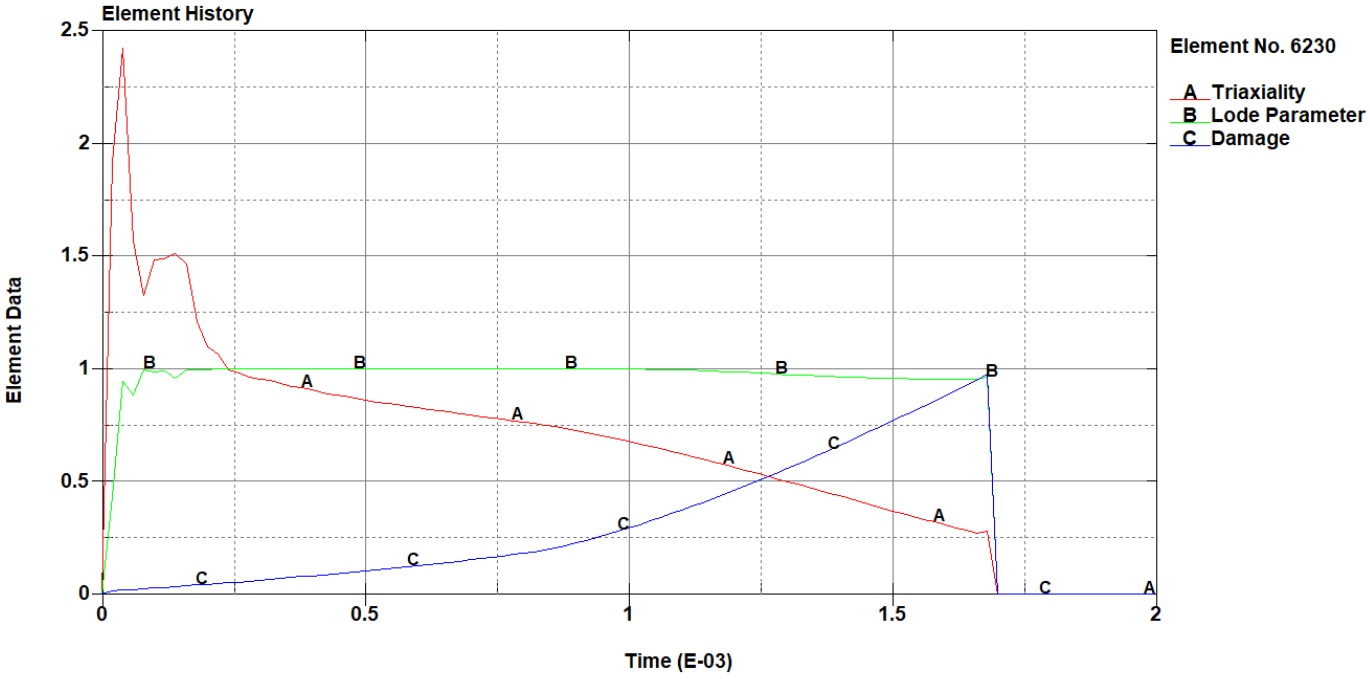

Figure 9: Applied pressure = 600 MPa. History plot of triaxiality (red), Lode parameter (green), and damage (blue) in the first element to fail (erode), located at the geometric center of the specimen's gage section. After 10% damage, the average triaxiality is about 0.65 (LS-DYNA definition) or -0.65 (standard definition), and the average Lode parameter is about 1.

The non-pressurized (0 MPa) case is used as a benchmark simulation. Figure 4 reveals damage localizing at the geometric center of the specimen gage section. Figure 5 illustrates a nearly constant triaxiality of about -0.33 (LS-DYNA definition) or 0.33 (standard definition), and Lode parameter of about 1, throughout the deformation history, indicative of proportional loading. These results are in good agreement with previous simulations of the same setup [27,31,45]. The pressurized (300 MPa and 600 MPa) cases are used to demonstrate how triaxiality can be tuned, at constant Lode parameter, by adjusting the applied pressure. For the 300 MPa case, the history plots in Fig. 7 reveal an average triaxiality of about 0.2 (LS-DYNA definition) or -0.2 (standard definition), and an average Lode parameter of about 1, with both averages commencing around 10% damage and concluding at the onset of fracture. The variation in triaxiality after 10% damage is acceptable but is not indicative of proportional loading. Significant oscillations in the stress state are observed prior to 10% damage, likely due to inertial (dynamic) effects associated with the sudden pressure jump at test startup. (Recall that the applied pressure was initiated as a step function at time $t = 0$, synchronous with the onset of uniaxial actuation.) For the 600 MPa case, the history plots in Fig. 9 reveal an average triaxiality of about 0.65 (LS-DYNA definition) or -0.65 (standard definition), and an average Lode parameter of about 1, with both averages commencing around 10% damage and concluding at the onset of fracture. The variation in triaxiality after 10% damage is acceptable but does not point toward proportional loading. Significant oscillations in the stress state are again observed prior to 10% damage. In all of our simulations, contour plots of the triaxiality and Lode parameter reveal that both are uniform over a large portion of the specimen gage section, a positive indicator of test repeatability.

Summary and Conclusions

Recent experiments have suggested (a) the potentially unanticipated importance of the negative triaxiality (compressive) region of Lode-triaxiality space in ductile fracture modeling and (b) the need to revisit previous interpretations of the "cut-off" value of the triaxiality, beyond which fracture cannot occur. As a first step toward addressing these needs, this paper presented a novel physical interpretation of the Lode parameter = 1 (constant) meridian over a range of triaxialities, spanning positive (tensile) to negative (compressive). Guided by this physical insight, ductile fracture experiments that employ hydrostatic pressure superposed on uniaxial tension were proposed and numerically simulated in LS-DYNA, with initial efforts focusing on 2024-T351 aluminum. Our numerical simulations provided a promising proof-of-concept, explicitly demonstrating tunability of the triaxiality between 0.33 (uniaxial tension) and -0.65 (equi-biaxial tension) at a constant Lode parameter of 1, accomplished by adjusting the magnitude of the applied pressure between 0 MPa and 600 MPa. For each of the simulated cases (0 MPa, 300 MPa, 600 MPa), our metrics for a "successful" test were met, which included (a) obtaining targeted values of triaxiality and Lode parameter, (b) holding these values "acceptably" constant over the duration of the simulation, and (c) ensuring these values are uniform over a large section of the specimen gage. Ongoing efforts are focused on suppressing the oscillatory response observed prior to 10% damage, likely due to inertial (dynamic) effects associated with the sudden pressure jump at test startup. One proposed solution is to perform a static initialization of the pressure implicitly prior simulating dynamic actuation explicitly. Overall, we feel that the proposed concept, with its embedded tunability, shows great promise for accessing a wide variety of stress states with a single experimental test setup.

Acknowledgments

This research was supported by the United States Federal Aviation Administration (FAA) under Cooperative Agreement No. 692M151940011. RLL is grateful to Bill Emmerling and Dan Cordasco for their support and involvement in the project. RLL would like to thank Jeremy Seidt and Amos Gilat for providing a CAD drawing of the candidate test specimen. RLL appreciates the constructive feedback provided by Paul Du Bois and Kelly Carney on the numerical simulations. The authors gratefully acknowledge the use of Altair HyperMesh through an Ohio Supercomputer Center statewide users license (Project No. PNS0455) and high-performance computing resources at the University of Dayton.

References

[1] W. Emmerling, D. Altobelli, K. Carney, and M. Pereira. "Development of a new material model in LS-DYNA – Part 1: FAA, NASA, and industry collaboration background." FAA Report No. DOT/FAA/TC-13/25 P1, 2014.

[2] D. Cordasco, W. Emmerling, and P. Du Bois. "A status review of failure simulation at the Federal Aviation Administration." In *Proceedings of the 11th European LS-DYNA Conference*, 2017.

[3] F.A. McClintock. "A criterion for ductile fracture by the growth of holes." *ASME J. Appl. Mech.* 35(2), 363–371, 1968.

[4] J.R. Rice and D.M. Tracey. "On the ductile enlargement of voids in triaxial stress fields." *J. Mech. Phys. Solids* 17(3), 201–217, 1969.

[5] A.L. Gurson. "Continuum theory of ductile rupture by void nucleation and growth. Part I: Yield criteria and flow rules for porous ductile media." *J. Eng. Mater. Technol.* 99(1), 2–15, 1977.

[6] V. Tvergaard and A. Needleman. "Analysis of the cup-cone fracture in a round tensile bar." *Acta Metall.* 32, 157–169, 1984.

[7] T. Pardoen and J.W. Hutchinson. "An extended model for void growth and coalescence." *J. Mech. Phys. Solids* 48, 2467–2512, 2000.

[8] A. Benzarga, J. Besson, and A. Pineau. "Anisotropic ductile fracture. Part II: Theory." *Acta Mater.* 52, 4639–4650, 2004.

[9] K. Nahshon and J. Hutchinson. "Modification of the Gurson model for shear failure." *Eur. J. Mech. A/Solids* 27, 1–17, 2008.

[10] G.R. Johnson and W.H. Cook. "Fracture characteristics of three metals subjected to various strains, strain rates, temperatures and pressures." *Eng. Fract. Mech.* 21(1), 31–48, 1985.

[11] J.W. Hancock and A.C. Mackenzie. "On the mechanisms of ductile failure in high-strength steels subjected to multi-axial stress-states." *J. Mech. Phys. Solids* 24(2–3), 147–169, 1976.

[12] O.S. Hopperstad, T. Børvik, M. Langseth, K. Labibes, and C. Albertini. "On the influence of stress triaxiality and strain rate on the behaviour of a structural steel. Part I. Experiments." *Eur. J. Mech. A/Solids* 22(1), 1–13, 2003.

[13] T. Børvik, O.S. Hopperstad, and T. Berstad. "On the influence of stress triaxiality and strain rate on the behaviour of a structural steel. Part II. Numerical study." *Eur. J. Mech. A/Solids* 22(1), 15–32, 2003.

[14] Y. Bao and T. Wierzbicki. "On fracture locus in the equivalent strain and stress triaxiality space." *Int. J. Mech. Sci.* 46(1), 81–98, 2004.

[15] Y. Bao. "Dependence of ductile crack formation in tensile tests on stress triaxiality, stress and strain ratios." *Eng. Fract. Mech.* 72(4), 505–522, 2005.

[16] N. Bonora, D. Gentile, A. Pirondi, and G. Newaz. "Ductile damage evolution under triaxial state of stress: theory and experiments." *Int. J. Plast.* 21(5), 981–1007, 2005.

[17] D. Mohr and S. Henn. "Calibration of stress-triaxiality dependent crack formation criteria: a new hybrid experimental-numerical method." *Exp. Mech.* 47(6), 805–820, 2007.

[18] I. Barsoum and J. Faleskog. "Rupture mechanisms in combined tension and shear — Experiments." *Int. J. Solids Struct.* 44(6), 1768–1786, 2007.

[19] L. Xue. "Damage accumulation and fracture initiation in uncracked ductile solids subject to triaxial loading." *Int. J. Solids Struct.* 44(16), 5163–5181, 2007.

[20] Y. Bai and T. Wierzbicki. "A new model of metal plasticity and fracture with pressure and Lode dependence." *Int. J. Plast.* 24, 1071–1096, 2008.

[21] K.S. Carney, P.A. Du Bois, M. Buyuk, and S. Kan. "Generalized, three-dimensional definition, description, and derived limits of the triaxial failure of metals." *ASCE J. Aerosp. Eng.* 22(3), 280–286, 2009.

[22] Y. Bai and T. Wierzbicki. "Application of extended Mohr-Coulomb criterion to ductile fracture." *Int. J. Fract.* 161, 1–20, 2010.

[23] T.B. Stoughton and J.W. Yoon. "A new approach for failure criterion for sheet metals." *Int. J. Plast.* 27(3), 440–459, 2011.

[24] K. Danas and P. Ponte Castaneda. "Influence of the Lode parameter and the stress triaxiality on the failure of elastic-plastic porous materials." *Int. J. Solids Struct.* 49, 1325–1342, 2012.

[25] L. Malcher and E.N. Mamiya. "An improved damage evolution law based on continuum damage mechanics and its dependence on both stress triaxiality and the third invariant." *Int. J. Plasticity* 56, 232–261, 2014.

[26] D. Mohr and S.J. Marcadet. "Micromechanically-motivated phenomenological Hosford-Coulomb model for predicting ductile fracture initiation at low stress triaxialities." *Int. J. Solids Struct.* 67-68, 40–55, 2015.

[27] J.D. Seidt. *Plastic Deformation and Ductile Fracture of 2024-T351 Aluminum Under Various Loading Conditions*. Ph.D. Dissertation, The Ohio State University, 2010.

[28] S.S. Haltom, S. Kyriakides, and K. Ravi-Chandar. "Ductile failure under combined shear and tension." *Int. J. Solids Struct.* 50, 1507–1522, 2013.

[29] J. Faleskog and I. Barsoum. "Tension-torsion fracture experiments – Part I: Experiments and a procedure to evaluate the equivalent plastic strain." *Int. J. Solids Struct.* 50, 4241–4257, 2013.

[30] A. Ghahremaninezhad and K. Ravi-Chandar. "Ductile behavior in polycrystalline aluminum alloy Al 6061-T6 under shear dominant loading." *Int. J. Fract.* 180, 23–39, 2013.

[31] J.D. Seidt. "Development of a new metal material model in LS-DYNA – Part 3: Plastic deformation and ductile fracture of 2024 aluminum under various loading conditions." FAA Report No. DOT/FAA/TC-13/25 P3, 2014.

[32] J.T. Hammer. "Plastic deformation and ductile fracture of Ti-6Al-4V under various loading conditions." FAA Report No. DOT/FAA/TC-TT14/2, 2014.

[33] J. Papasidero, V. Doquet, and D. Mohr. "Ductile fracture of aluminum 2014-T351 under proportional and non-proportional multi-axial loading: Bao-Wierzbicki results revisited." *Int. J. Solids Struct.* 69-70, 459–474, 2015.

[34] M. Scales, N. Tardif, and S. Kyriakides. "Ductile failure of aluminum alloy tubes under combined torsion and tension." *Int. J. Solids Struct.* 97-98, 116–128, 2016.

[35] M. Scales, K. Chen, and S. Kyriakides. "Material response, localization, and failure of an aluminum alloy under combined shear and tension: Part I experiments." *Int. J. Plast.*, https://doi.org/10.1016/j.ijplas.2019.04.004, 2019.

[36] Y. Bao Y and T. Wierzbicki T. "On the cut-off value of negative triaxiality for fracture." *Eng. Fract. Mech.* 72(7), 1049–1069, 2005.

[37] S. Haight, L. Wang, P. Du Bois, K. Carney, and C.D. Kan. "Development of a titanium alloy Ti-6Al-4V material model used in LS-DYNA." FAA Report No. DOT/FAA/TC-15/23, 2016.

[38] A.S. Khan and H. Liu. "A new approach for ductile fracture prediction on Al 2024-T351 alloy." *Int. J. Plast.* 35, 1–12, 2012.

[39] Y. Lou, J.W. Yoon, and H. Huh. "Modeling of shear ductile fracture considering a changeable cut-off value for stress triaxiality." *Int. J. Plast.* 54, 56–80, 2014.

[40] P. Kubik, F. Sebek, J. Hulka, and J. Petruska. "Calibration of ductile fracture criteria at negative stress triaxiality." *Int. J. Mech. Sci.* 108-109, 90–103, 2016.

[41] M. Brunig, S. Gerke, and M. Schmidt. "Damage and failure at negative stress triaxialities: Experiments, modeling and numerical simulations." *Int. J. Plast.* 102, 70–82, 2018.

[42] P.W. Bridgman. *Studies in Large Plastic Flow and Fracture.* Harvard University Press, Cambridge, MA, 1964.

[43] J.J. Lewandowski and P. Lowhaphandu. "Effects of hydrostatic pressure on mechanical behaviour and deformation processing of materials." *Int. Mater. Rev.* 43(4), 145–187,1998.

[44] J.D. Seidt, personal communication, 3 April 2020.

[45] C.K. Park, K. Carney, P. Du Bois, D. Cordasco, and C.D. Kan. "Aluminum 2024-T351 input parameters for MAT_224 in LS-DYNA. FAA Report No. DOT/FAA/TC-19/41, 2020.